Available online at www.sciencedirect.com
ScienceDirect
Journal of the European Ceramic Society 27 (2007) 2137–2143
www.elsevier.com/locate/jeurceramsoc

Corrosion of β-sialon-based ceramics by molten steel

J. Křest'an [a,*], O. Pritula [a], Ľ. Smrčok [a], P. Šajgalík [a], Z. Lenčéš [a], A. Wannberg [b], F. Monteverde [c]

[a] *Institute of Inorganic Chemistry, Slovak Academy of Sciences, Dúbravská cesta 9, SK-845 36 Bratislava, Slovak Republic*
[b] *Studsvik Neutron Research Laboratory, Uppsala University, SE-611 82 Nyköping, Sweden*
[c] *Institute of Science and Technology for Ceramics, National Research Council, Via Granarolo 64, 48018 Faenza, Italy*

Received 14 April 2006; received in revised form 27 July 2006; accepted 7 August 2006
Available online 2 October 2006

Abstract

The corrosion resistance of sialons made from commercial powders (AlN, Al_2O_3 and Si_3N_4) and from powder precursor produced by carbothermal reduction and nitridation of raw aluminosilicate (pyrophyllite) in molten steel were investigated. The corroded zone in sialon made from raw pyrophyllite (P1) is more then two times deeper compared to the corroded zone of sialon made from commercial powders (C1). The corrosion zone of sample P1 is on the average 610 μm deep, while in sample C1 it is only 260 μm. The main corrosion products are γ-Al_2O_3 and iron silicides. The phase compositions were estimated by neutron Rietveld refinement.

Keywords: Corrosion; Sialon; Steel

1. Introduction

Recently the application of advanced ceramics increases also in the metallurgical industry, consequently the knowledge of their corrosion behaviour is essential.[1,2] β-Sialon ($Si_{6-z}Al_zO_zN_{8-z}$; $0<z<4.3$) ceramics are frequently used materials in the industry owing to their good mechanical properties and reasonable price. For engineering application in steel industry the knowledge of corrosion behaviour in molten steel is important. However, a search in commonly available literature quickly revealed that the data on this subject are rather scarce. Among them, the wettability of sialon-based ceramics by molten steel has been investigated by Amadeh et al.,[3] who reported a good corrosion resistance of carbon doped β-sialon against molten steel. Interaction and reaction mechanism of Si_3N_4 with carbonyl iron in nitrogen or argon atmosphere was discussed by Shimoo et al.[4] They found that Fe–Si solid solutions were formed both in nitrogen and in argon. With increasing temperature the corrosion products were iron silicides in the following order of occurrence: Fe_3Si, Fe_5Si_3 and FeSi.

β-Sialon ceramics are usually prepared by reactive sintering of appropriate mixtures of Si_3N_4, Al_2O_3 and AlN powders. The aim of present paper was to test the corrosion resistance of two types of β-sialons against molten steel: the first prepared from commercial powders, and the second one from precursors synthesised by carbothermal nitridation of pyrophyllite. Model experiments were also carried out to reveal the phase composition of corrosion products.

2. Experimental

Two types of bulk sialon-based ceramic materials with parameter $z=3.7$ were prepared: β-sialons made from commercial powders (AlN, Al_2O_3 and Si_3N_4) and from powder precursor produced by carbothermal reduction and nitridation of raw aluminosilicate, pyrophyllite with ideal composition $Al_2Si_4O_{10}(OH)_2$. The powder materials used in this work were pyrophyllite (P-I, Envigeo s.r.o., Slovakia), α-Al_2O_3 (Martoxide PS-6, Martinswerk, FRG), α-Si_3N_4 (Siconide-P, Permascand Ceramic, Sweden), β-Si_3N_4 (Tschernogolovka, Russia), AlN (Grade C, H.C. Starck, Germany) and carbon black (Stickstoffwerk Piesteritz, Germany). The chemical compositions of the pyrophyllite according to Envigeo s.r.o., are given in Table 1. The pyrophyllite powder was ground in planetary mill for 0.5 h

* Corresponding author.
E-mail address: uachkjan@savba.sk (J. Křest'an).

0955-2219/$ – see front matter © 2006 Elsevier Ltd. All rights reserved.
doi:10.1016/j.jeurceramsoc.2006.08.012

Table 1
Chemical composition of pyrophyllite P-I (according Envigeo, s.r.o.)

P-I	wt.%
SiO_2	78.23
TiO_2	0.59
Al_2O_3	15.85
Fe_2O_3	1.65
CaO	0.23
MgO	<0.01
MnO	0.02
Na_2O	0.02
K_2O	0.03
P_2O_5	0.10
Loss of ignition	3.11
H_2O	0.29

and sieved through 70 μm screen. The compositions of starting powder mixtures are summarised in Table 2. The appropriate amount of dry powder materials was homogenized on a roller in a PE bottle for 4 h using alumina balls. The homogenized powder mixture was poured into the static graphite reactor, which was inserted into a graphite resistance furnace. The reactor was kept under vacuum up to 600 °C, above this temperature nitrogen gas was introduced through a diffuser into the reactor. The temperature was measured by W5Re/W25Re thermocouple up to 1100 °C. A two-colour pyrometer (Ircon, USA), calibrated by gold (1063 °C), diopside (1392 °C) and alumina (2045 °C) was used for the temperature measurement of the reactor surface above 1100 °C. The final temperature of carbothermal reduction and nitridation (CRN) was 1510 °C with 8 h dwell at this temperature. The nitrogen flow (100 $cm^3\ min^{-1}$) was controlled by means of calibrated flowmeter. The products of CRN were analyzed by XRD (Stoe STADI-P, Co $K\alpha_1$) and SEM (Jeol JSM 35) methods.

The powder products of CRN were pressed into pellets in a steel die at 100 MPa. The compacted samples were hot-pressed (HP) in a graphite die at 1750 °C for 2 h in 0.1 MPa of nitrogen and mechanical load of 30 MPa (sample P1). For a comparison, the mixture C1 with parameter $z = 4$ was prepared from commercially available Si_3N_4, AlN and Al_2O_3 powders and hot-pressed under the same conditions. The XRD and SEM methods were used to analyse the samples after high temperature treatment. The z value as the mean of z_a and z_c was calculated according to the following equations (standard deviations within parentheses)[5]:

$$a\,(\text{Å}) = 7.603(6) + 0.0297(4)z_a$$

$$c\,(\text{Å}) = 2.907(8) + 0.0255(6)z_c$$

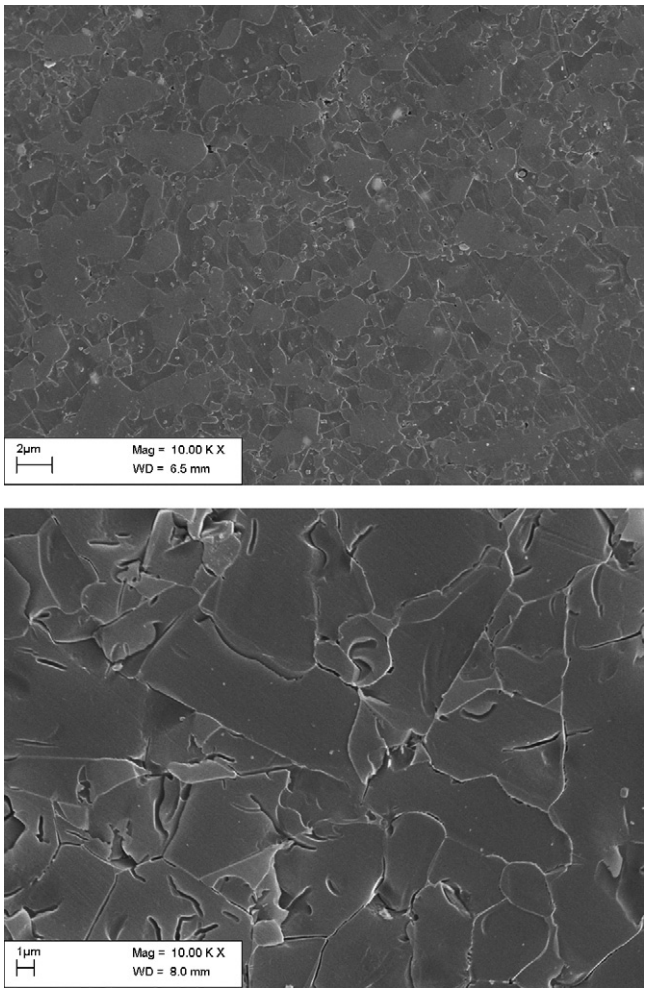

Fig. 1. The microstructures of samples C1 (up) and P1 (down) after chemical etching.

The subscripts indicate the z value calculated from a and c lattice parameters of the hexagonal sialon, respectively.[6] Microstructure of sintered samples were analyzed by SEM after chemical etching by 85% solution of H_3PO_4.

For corrosion test sialon cuboids (samples C1, P1) were placed into a corundum crucible and dusted with an excess of steel sawdust (CSN 11523), and annealed in graphite resistance furnace. After heat treatment at 1700 °C for 2 h in Ar atmosphere polished cross-sections of the corroded samples were prepared, and analyzed using SEM (Leica Cambridge, S360, UK) equipped with EDX (INCA Energy 300, Oxford Instruments Analyt., UK).

Model corrosion tests were also carried out to find the final corrosion products. Samples C1S (i.e. C1 + steel) and P1S

Table 2
Composition of starting mixtures

Sample	Pyrophyllite P-I (wt.%)	Carbon black (wt.%)	β-Si_3N_4 (wt.%)	α-Al_2O_3 (wt.%)	α-Si_3N_4 (wt.%)	AlN (wt.%)
P1[a]	53.5	25.8	5.2	15.5		
C1				47.9	32.9	19.2

[a] Theoretical composition corresponds to the value $z = 4$ after addition of 37.7 wt.% of α-Al_2O_3 to the 62.3 wt.% of P1 after carbothermal reduction and ntiridation.

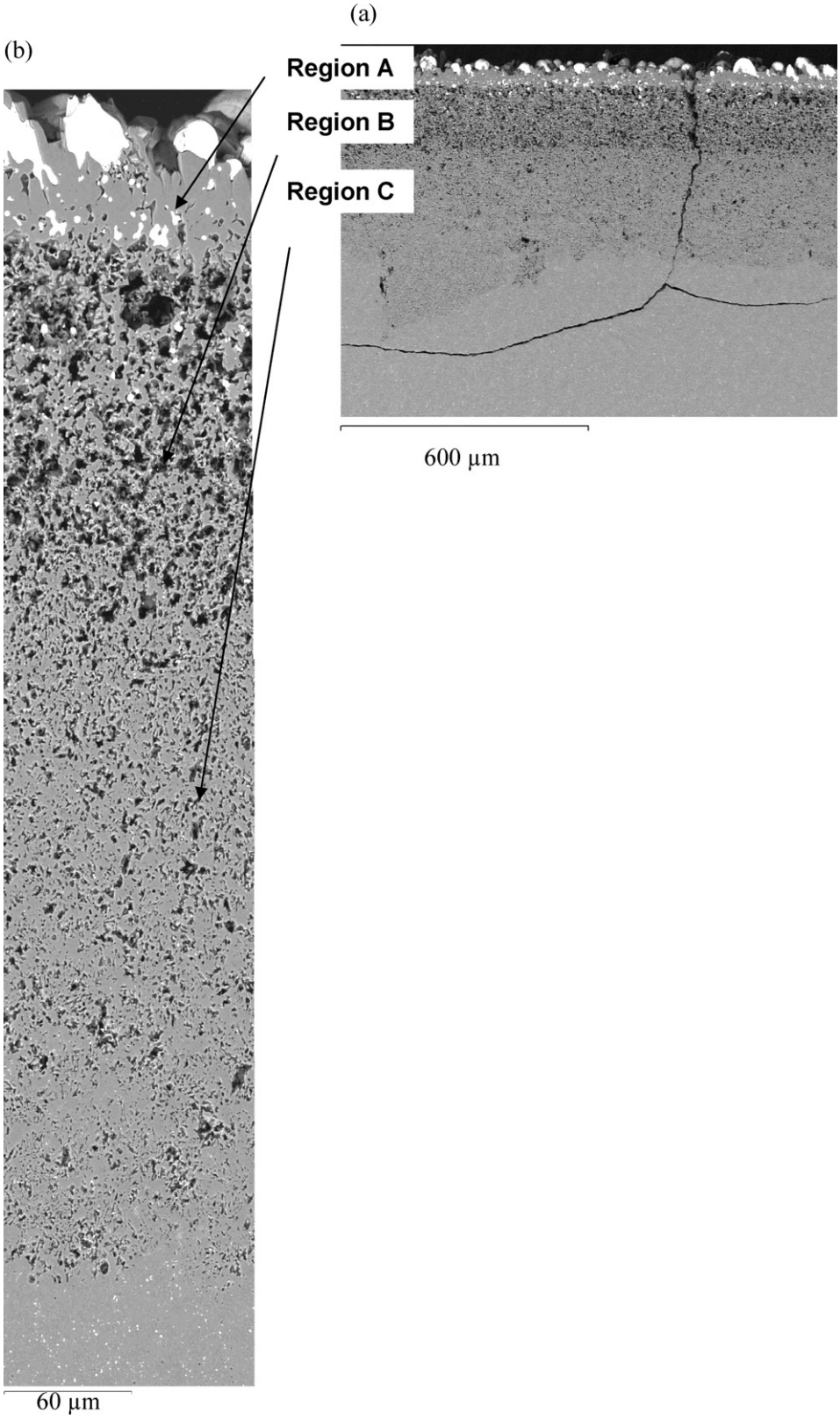

Fig. 2. The cross-section of the sialon sample P1 after static corrosion at 1750 °C for 2 h in argon with visible corrosion regions.

(P1 + steel) were prepared by homogenization of C1 and P1 sialon powders and 20 wt.% of steel sawdust (CSN 11523) in a planetary ball mill. The mixtures were compacted by cold isostatic pressing (CIP) and heat treated at 1700 °C for 2 h in Ar atmosphere.

All four samples (C1, P1, C1S, P1S) were crushed and analyzed with STOE Stadi P diffractometer (10–80° 2Θ) equipped with a linear PSD and a curved Ge(1 1 1) primary beam monochromator. Neutron diffraction patterns of all samples were collected on the R2D2 diffractometer installed in the Neutron Research Laboratory, Studsvik, using the wavelength of 1.5518 Å. The samples were placed into vanadium containers.

Phase analysis was done by Rietveld refinements based on the following crystal structures: β-sialon (space group $P6_3/m$),[7] α-Al_2O_3 ($R-3c$),[8] SiC ($F-43m$),[9] γ-Al_2O_3 ($Fd-3m$),[10] Fe_5Si_3 ($P6_3/mcm$),[11] Fe_3Si ($Fm3m$)[12] and FeSi ($P2_13$).[13] All Rietveld refinements were done using the FullProf program.[14] The strategy of all refinements was based on a stepwise addition of relevant phases starting with the most abundant and proceeding towards the phase with the smallest expected weight fraction. Due to complexity of the system the atomic parameters were not relaxed.

3. Results and discussion

The microstructures of samples C1 and P1 after chemical etching are shown in Fig. 1. Samples were etched by 85% solution of H_3PO_4, which react preferentially with the silicate rich

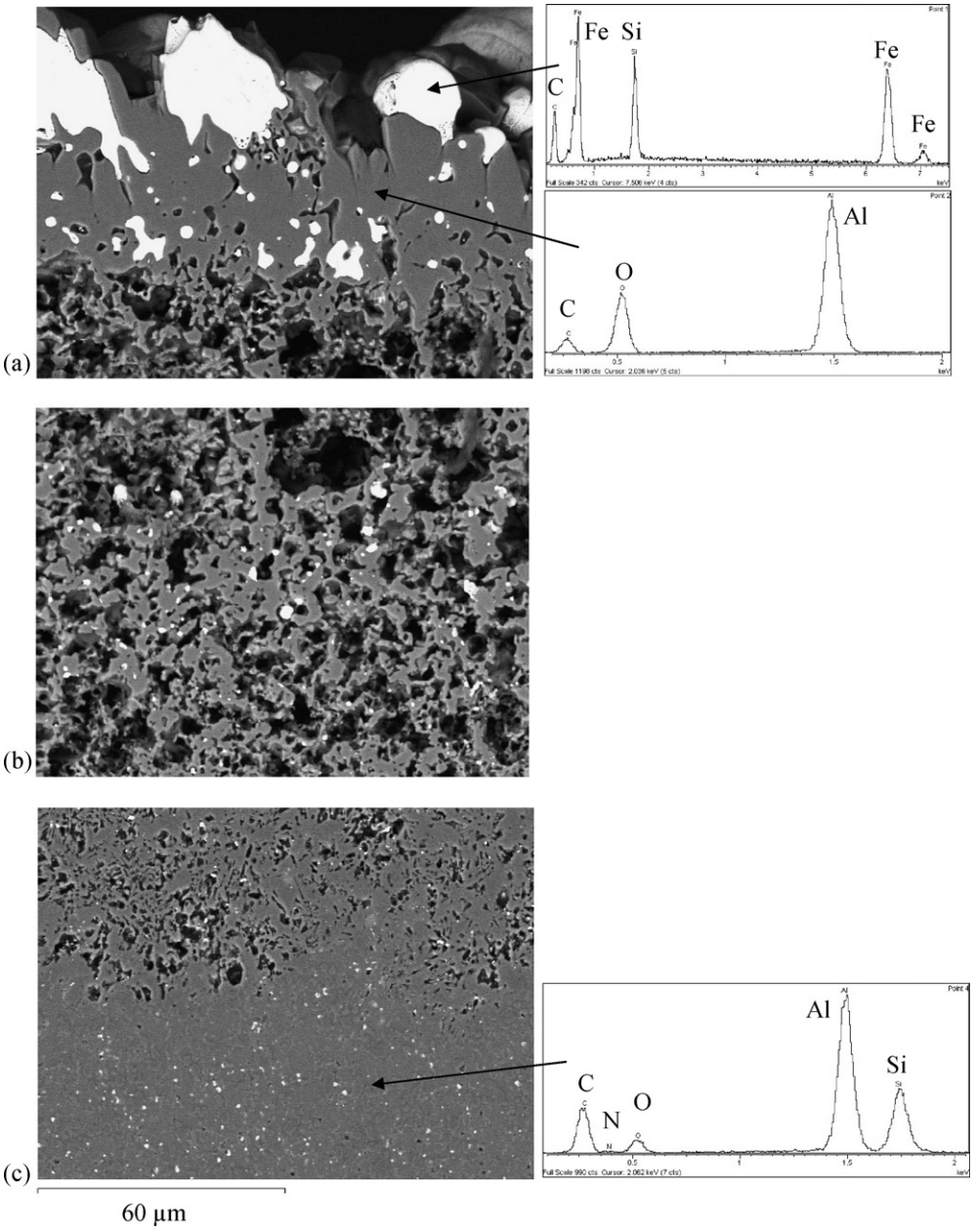

Fig. 3. Detailed SEM micrograph of the corrosion regions of sample P1.

grain boundary phases. From the microphotographs in Fig. 1 is visible that sample P1 have more etched grain boundary and thus more grain boundary phases compared to sample C1.

The polished cross-section of the sialon samples after static corrosion at 1700 °C for 2 h in argon is shown in Figs. 2–4. Sample P1 has more than two times thicker corroded zone compared to sample C1. Sample P1 shows a corroded zone noticeably thicker than sample C1 (∼610 μm *versus* ∼260 μm). Moreover, macrocracking accompanied the corrosion of sample P1 (Fig. 2a).

3.1. Sample P1

The corrosion region of sample P1 can be divided into three areas (Fig. 2). The sample surface is covered by a compact 70 μm thick layer, region A. This layer consists of two different phases, the continuous grey matrix and a globular white minor phase. The region B is up to the depth of 230 μm, and is characterized by a large porosity. This region contains small white spheres in the upper part of the porous area. In the last region C, the porosity continuously decreases. Finally, in the depth of 610 μm only the original sialon can be observed.

A more detailed study of the boundary between the sialon and region C (Fig. 3c) showed, that the grains keep their original needle-like shape. The microstructure looks like the one formed after chemical etching and thus it can be argued that the corrosion starts along the grain boundaries (Fig. 3c). A micrograph taken from the upper part of region B (Fig. 3b) shows that elongated grains are vanishing due to the corrosion and the porosity increases. In this region even the sialon grains were partly dissolved. Towards the surface of the sample the porosity increased and the white spheres appeared, probably as a result of the corrosion reactions. The largest pores are visible just beneath the dense layer. The relatively dense continuous surface layer (region A) contains white separated areas. The boundary between the grey and white phase is sharp, without any visible interphase. On the outermost surface of the sample individual areas of white phase are visible.

EDX analysis of the upper continuous layer revealed that the white spots contained iron and silicon (with high probability iron silicides), and the grey layer consisted of aluminum and oxygen.

3.2. Sample C1

Fig. 4a shows the cross-section of sample C1. The corrosion layer can be again divided into three parts. Contrary to the sample P1, region C is smaller; region B is similar in size (up to depth of 170 μm), but from the compositional point of view it

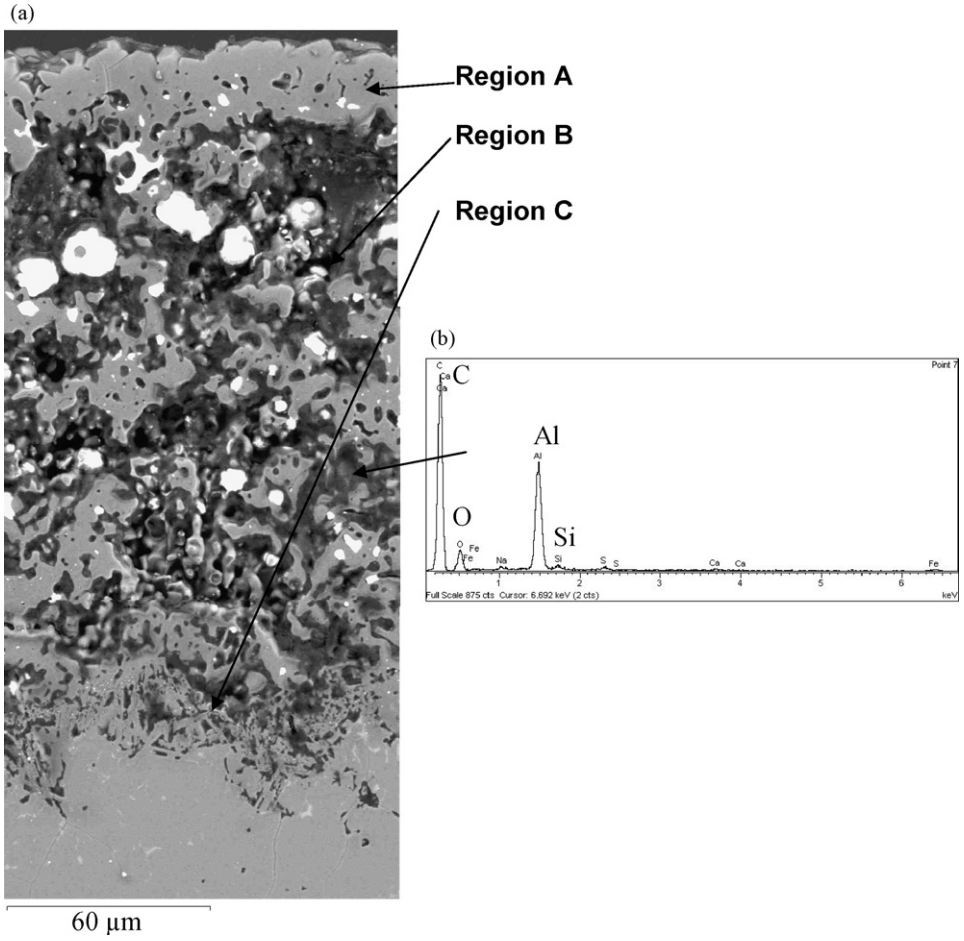

Fig. 4. The cross-section of the sialon sample C1 after static corrosion at 1750 °C for 2 h in argon with depicted corrosion regions.

seems to be more complex. Region A is thinner (30 μm) and contains lower amount of white phase compared to sample P1. The grain boundary phase was etched out and the original β-sialon grains are clearly visible in this region. EDX analysis again suggested that the white spheroids, mainly in the region B are most probably iron silicides and the upper continuous grey layer is alumina. Within the region B, except for Al, O elements, an increased intensity of C peak was detected (Fig. 4b), in contrast to the sample P1. However, the quantification of carbon is difficult, because the samples were coated by carbon before the EDX analysis.

3.3. Model experiments

In order to simulate the corrosion process two more samples, C1S and P1S, were prepared. Both compositions were treated at the same conditions as the static corrosion tests were performed. The aim of these experiments was to check the phase composition of corrosion products by means of XRD and neutron diffraction.

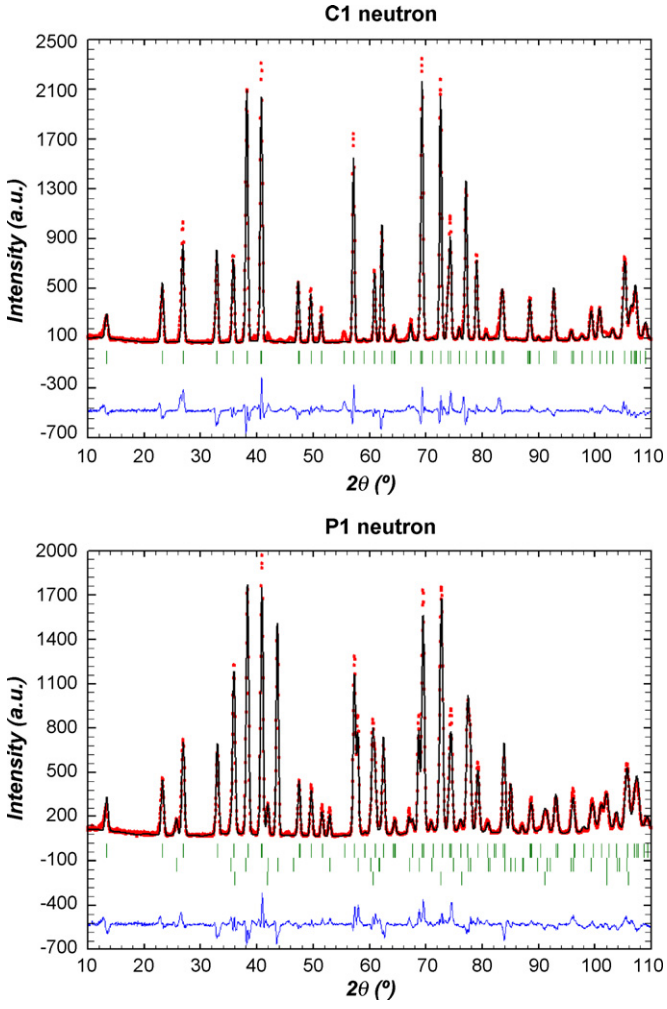

Fig. 5. Rietveld fit of the neutron pattern of P1 and C1 sialons after HP at 1750 °C for 2 h in nitrogen atmosphere with fixed atomic parameters. The markers of the Bragg positions below the X-ray pattern from top to bottom correspond to β-sialon in sample C1 and β-sialon, α-Al_2O_3 and β-SiC in sample P1.

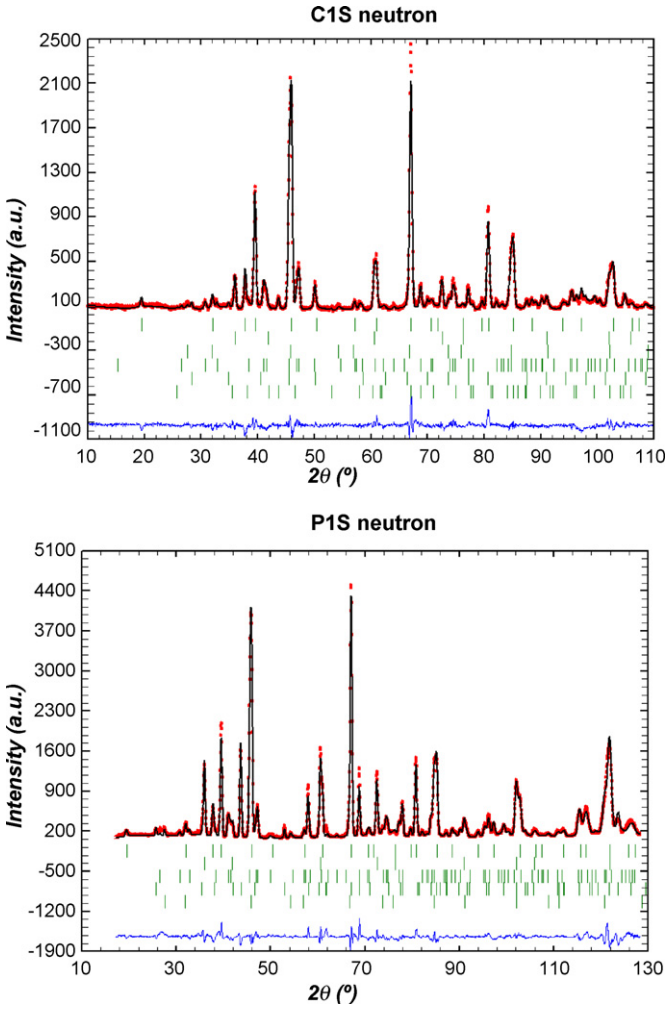

Fig. 6. Rietveld fit of the neutron pattern of corroded model mixtures (sample P1S and C1S) after corrosion test at 1700 °C for 2 h in argon atmosphere with fixed atomic parameters. The markers of the Bragg positions below the X-ray pattern from top to bottom correspond to γ-Al_2O_3, Fe_3Si, Fe_5Si_3, FeSi, β-SiC and α-Al_2O_3 in sample C1S and γ-Al_2O_3, Fe_5Si_3, Fe_3Si, β-SiC and α-Al_2O_3 in sample P1S.

Fig. 5 shows the neutron diffraction patterns of P1 and C1 sialons before the corrosion test. Sample C1 is in fact a pure β-sialon, while sample P1 contains also some amount of α-alumina and β-SiC. α-Al_2O_3 is a residuum of non-reacted α-alumina from the starting mixture, and SiC is formed during the carbothermal reduction and nitridation of pyrophyllite powder.[6] The neutron diffraction patterns of corroded model mixtures are shown in Fig. 6. It is seen, that in both cases sialon is not present. The major phase detected in the C1S sample was γ-Al_2O_3. This phase is probably the grey phase in the surface layer of sample C1S after corrosion test (Fig. 4). Moreover, β-SiC, FeSi, Fe_3Si, Fe_5Si_3 phases and minor amount of α-Al_2O_3 were identified. Analysis of the sample P1S, with the exception of FeSi, revealed the same phases as in the C1S case. The amount of α-Al_2O_3 and β-SiC was however higher, as they were already present in the starting material. The quantitative phase analysis of all samples obtained from neutron diffraction patterns by Rietveld analysis are given in Table 3.

Table 3
The quantitative phase analysis obtained from the neutron diffraction patterns by Rietveld analysis

Sample	β-Sialon (wt.%)	γ-Al_2O_3 (wt.%)	β-SiC (wt.%)	α-Al_2O_3 (wt.%)	FeSi (wt.%)	Fe_3Si (wt.%)	Fe_5Si_3 (wt.%)	R_{wp}
C1	100	–	–	–	–	–	–	0.20
P1	60	–	9	31	–	–	–	0.14
C1S	–	53	5	2	9	11	21	0.17
P1S	–	42	11	17	–	15	15	0.15

3.4. Discussion

On the basis of the obtained results we propose that the corrosion of β-sialon by steel proceeds in two steps. Step 1: reaction between the liquid steel and the silicate-based grain boundary phase of β-sialon. The main products of these reactions in graphite resistance furnace and in the graphite crucibles, where the activity of carbon must be also taken into account, are iron silicides and β-SiC. This step might be responsible for the appearance of β-sialon grains located on the interface between the original β-sialon bulk and corroded region C.

Step 2: the β-sialon grains also start to react with the liquid steel. Reaction between sialon ($Si_{2.3}Al_{3.7}O_{3.7}N_{4.3}$) and liquid steel produces γ-Al_2O_3, iron silicides and small amount of α-Al_2O_3 as solid products. Some gaseous species like Al_2O, CO and N_2 are also evolved due to the presence of carbon in the reaction system. The formation of gaseous species can be documented by the round shaped pores; their size increased towards the surface of the sample.

From the micrographs in Figs. 3 and 4 it can be seen that in the region B in both P1 and C1 samples, the system was molten and from this melt spheroids of iron silicides were formed. The eutectic temperatures of iron silicides are in the range of 1196–1215 °C, well below the temperatures used during the corrosion tests. The top layer consists of continuous γ-Al_2O_3 layer, which was probably formed from the melt mentioned above during cooling. In the case of sample P1 the corroded layer contains several cracks perpendicular to the surface. Moreover, parallel cracks beneath the corroded region are present (Fig. 2). All that cracking is probably caused by the difference in thermal expansion coefficients of β-sialon and γ-Al_2O_3.

4. Conclusions

The β-silaon prepared from commercial powders (C1) showed better corrosion resistance compared to pyrophyllite derived one (P1). The corroded zone P1 sialon is more then two times deeper compared to the corroded zone of C1 sialon. The average thickness of corrosion zone is 610 μm (P1) and 260 μm (C1), respectively. The corroded zone can be divided to three different regions in both samples with different porosity and phase composition.

The solid products of the model corrosion experiments of sialon composite made from raw pyrophyllite (P1S) are γ-Al_2O_3, Fe_3Si, Fe_5Si_3, β-SiC, and α-Al_2O_3. The same corrosion products were observed in the case of sialon made from commercial powders (C1S), although in different quantities. In addition, 9% of FeSi was detected.

Acknowledgements

Work was supported by the Slovak Grant Agency, project nos. VEGA 2/4072/24, APVT-51-049702, Centrum of Excellence NANOSMART and by the Alexander von Humboldt Foundation, Germany.

References

1. Riley, F. L., *Key Eng. Mater.*, 1996, **113**, 1–14.
2. Dower, L. T. and Coley, K., *Key Eng. Mater.*, 1996, **113**, 167–176.
3. Amadeh, A. A., Labbe, J. C. and Quintard, P. E., *J. Eur. Ceram. Soc.*, 2005, **25**, 1041–1048.
4. Shimoo, T., Yamasaki, T. and Okamura, K., *J. Ceram. Soc. Jpn.*, 1997, **105**(9), 734–739.
5. Ekström, T., Käll, P. O., Nygren, M. and Olssen, P. O., *J. Mater. Sci.*, 1989, **24**, 1853–1861.
6. Křest'an, J., Šajgalík, P. and Pánek, Z., *J. Eur. Ceram. Soc.*, 2004, **24**, 791–796.
7. van Dijen, F. K., Metselaar, R. and Helmholdt, R. B., *J. Mater. Sci. Lett.*, 1987, **6**, 1101–1102.
8. Brown, A. S., Spackman, M. A. and Hill, R. J., *Acta Cryst. A*, 1993, **49**, 513–527.
9. Kawamura, T., *Mineral. J. (Jpn.)*, 1965, **4**, 333–355.
10. Smrčok, Ľ., Langer, V. and Křest'an, J., *Acta Cryst. C*, 2006, **62**, i83–i84.
11. Weill, A. R., *Nature (Lond.)*, 1943, **152**, 413.
12. Schütte, M., Wartchow, R. and Binnewis, M., *Z. Anorg. Allg. Chem.*, 2003, **629**, 1846–1850.
13. Wood, I. G., David, W. I. F., Hull, S. and Price, G. D., *J. Appl. Cryst.*, 1996, **29**, 215–218.
14. Rodriguez-Carvajal, J., *FullProf*, 2000, http://www-llb.cea.fr/fullweb/fp2k/fp2k.htm.